Influence of processing parameters on creep and recovery behavior of FDM manufactured part using definitive screening design and ANN

Article *in* Rapid Prototyping Journal · October 2017

DOI: 10.1108/RPJ-12-2015-0198

CITATIONS
30

READS
909

3 authors:

Omar Ahmed Mohamed
Deakin University
47 PUBLICATIONS **1,468** CITATIONS

SEE PROFILE

S. H. Masood
Swinburne University of Technology
250 PUBLICATIONS **6,531** CITATIONS

SEE PROFILE

Jahar Bhowmik
Swinburne University of Technology
74 PUBLICATIONS **784** CITATIONS

SEE PROFILE

Abstract

Purpose

The purpose of this paper is to investigate the effect of process parameters of Fused Deposition Modelling (FDM) 3D Printing process on viscoelastic responses (creep compliance and recoverable compliance) of FDM built parts using a novel experimental design technique.

Design/methodology/approach

As part of the process characterization, a recently developed class of three-level design methodology - definitive screening design - was employed in this study to fit a second order polynomial regression model. Artificial neural network (ANN) was also used to determine the optimal process parameters to improve creep compliance and recoverable compliance. The relationships between layer thickness, air gap, raster angle, build orientation, road width, number of contours and creep performance of FDM fabricated part were thereafter established empirically. Scanning electron microscope (SEM) is used to examine and characterize the morphology of the structures for some samples.

Findings

This study found that the creep resistance of FDM manufactured part is significantly influenced by layer thickness, air gap, raster angle and number of contours and it can be improved by optimizing the settings of the selected parameters. The relationship between FDM process parameters and creep properties was determined, with the best creep performance observed with using 0.127 mm of layer thickness, zero air gap, zero raster angle, build orientation of 17.188˚, road width of 0.4572 mm and 10 contours. Finally, the result is verified by confirmation experiments. The results prove that definitive screening design is very effective design in characterizing the influence of process parameters on creep properties of FDM built part at lowest cost.

Originality/value

The originality of this paper lies in characterizing and optimizing the effect of process parameters on creep performance of FDM manufactured part that has not been studied in all previous studies. The paper highlights for the first time how the application of definitive screening design (DSD) can overcome most of the limitations encountered in the conventional techniques. This study can be used as a guide to the different additive manufacturing users of various industries and the results provide a good technical database on how FDM process parameters influence the creep performance of manufactured parts.

1. Introduction

Fused Deposition Modeling (FDM) is one of the most widely used 3D printing technologies on the market for manufacturing prototypes in a wide range of thermoplastic materials since the 1980s. The FDM process is fast becoming the most popular and affordable additive manufacturing method to produce complex shapes at the lowest cost without needing any tooling (Mohamed et al., 2015). This technology is based on the extrusion of heated filament of thermoplastics through a small-diameter nozzle which has a mechanism to control the flow of the semi-molten filament to be turned on and off onto a platform vertically and horizontally to produce parts in a layer-by-layer manner from computer aided design (CAD) models (Masood, 2007). The efficiency and simplicity of the FDM technology have made it the best technology for various industries. Although it offers several advantages over traditional manufacturing processes such as injection moulding, when it comes to fabricating functional parts and strong structure having superior mechanical performance and properties, the advantages of FDM process is not so distinct due to it being characterized by the large number of interacting process parameters and complex optimal settings. Generally, the mechanical properties and performance of any material and the manufactured parts by FDM process change with increasing temperatures. Some properties and performance, such as flexural modulus, tensile strength, impact Strength and compression strength decrease with the increase in temperature. Other properties and performance such as creep increases with the increase in temperature.

Creep is an important characteristic in predicting the properties and performance of the manufactured part by FDM process in many industrial applications for long-term durability and reliability for survival under the applied load. As an inherent defect, creep deformation causes dimensional stability problems affecting the service durability and safety of the FDM manufactured parts, which is a major issue for their expansion of applications in many industries such as in automotive and aerospace engineering. Thus it has a severe effect on the product performance. Poor creep resistance of the FDM manufactured part is considered as a deficiency of the part functionality and is unfavorable to their applications for long-term loading. Creep in the manufactured part by FDM process is a complex phenomenon, which depends not only on the material used, but also on the process parameters and their interactions. By performing creep-recovery tests at the forming temperature, it is possible to predict whether the fabricated sample by FDM process and its structure has sufficient elasticity to maintain its shape and produce a stable product (i.e. low plastic deformation under load). For high performance and maximum lifetime, FDM built parts must have a high creep resistance (i.e. low deformation under load) under long-term loading.

A large number of studies on the characterization and optimization of FDM process parameters on mechanical strength have been made. Impens and Urbanic (Impens and Urbanic, 2015) carried out an experimental study on the influence of post-processing variables on tensile and compression strengths for 3D printed processed parts. This study revealed that build orientation has a critical impact on the part strength with or without the infiltration. Rayegani and Onwubolu (Onwubolu and Rayegani, 2014) examined the

influence of FDM process variables on tensile strength of part processed by FDM process using design of experiment, differential evolution (DE) and group method of data handling (GMDH). It was concluded that negative air gap, small raster road and zero build orientation greatly improve the tensile strength. Gajdoš et al. (Gajdoš et al., 2015) demonstrated that the sparse structure can be used to obtain weight reduction with sufficient flexural strength compared to the part properties manufactured with default machine settings. Durgun and Ertan (Durgun and Ertan, 2014) studied the effect of raster angle and part orientation on the mechanical properties and surface finish of FDM manufactured parts. Authors reported that the build orientation has a more significant effect than the raster angle on the mechanical properties. Lanzotti et al. (Lanzotti et al., 2015) recently conducted a study on the influence of process variables on ultimate tensile strength of PLA processed parts. From the experimental results it was found that the infill orientation, layer thickness and perimeters, significantly affect the ultimate tensile strength.

Recent years Artificial Neural Network (ANN) is attracting increasing attention as a predictive tool in various engineering applications, including additive manufacturing processes due to its capability to capture non-linear relationship between the process parameters and mechanical properties. Recently, a few researchers have implemented the artificial neural network to optimize FDM process parameters. For example, Peng et al. (Peng et al., 2014) optimized FDM process parameters for dimensional accuracy of the printed part using response surface methodology and ANN technique. Sood et al. (Sood et al., 2012b) investigated the impact of process variables on the compressive strength using empirical modeling and ANN technique. This study concluded that in order to maximize compressive strength, the part must be manufactured with less number of layers and shorter raster lengths. In another study, Sood et al. (Sood et al., 2010a) combined the ANN with bacterial foraging algorithm to determine the optimal process setting for mechanical properties of part built by FDM. Liangbo et al. focused on predicting the product precision in FDM using ANN and concluded that the developed ANN model has sufficient accuracy in predicting the product precision.

The existing literature has investigated the effect of processing parameters on the static mechanical properties of FDM manufactured part. However, the influence of FDM process conditions on the creep and recovery behaviors and time-dependent deformation has not been studied yet and the relationships between the FDM process parameters and creep properties are unknown. The aim of this study is to investigate the impact of processing parameters on creep and recovery properties of the manufactured parts by FDM process. The creep compliance and recoverable compliance were measured. This study also reports for the first time the application of a cost effective design, known as definitive screening design (DSD), in additive manufacturing processes to establish functional relationships between the process parameters and creep properties. The study involved six FDM process parameters for the characterization of creep and recovery behaviors. The optimal process conditions were also determined using artificial neural network (ANN).

2. Materials and methods

In the study Polycarbonate-acrylonitrile butadiene styrene (PC-ABS) specimens were fabricated using the Stratasys' Fortus 400 FDM machine. All specimens were manufactured having dimensions of 60 mm (length), 12.5 mm (width) and 3.5 mm (thickness) according to the Thermal Advantage Instrument (TAI) manufacturer recommendations (DMA2980, 2002), FDM equipment manufacturer (Stratasys) and real industrial applications. The standard Dynamic Mechanical Analysis (DMA) Model 2980TA Instrument was used to measure the creep and recovery performance of the FDM manufactured parts under different process conditions. Fig. 1 shows the arrangement of the DMA equipment and specimen clamping in a dual cantilever mode. In each test, the specimen was heated to the desired temperature of 80°C and was allowed to equilibrate for 3 minutes (soak time) prior to beginning the test in order to make sure that the specimen has reached the thermal equilibrium. In this test, the data sampling interval parameter of 0.2 second is used based on DMA machine type in order for the data to be plotted on a logarithmic scale. Stress sweep tests were conducted between 0.1 and 10 Hz to select the value of stress within the linear viscoelastic region (LVR). The creep compliance and recoverable compliance were measured for the specimen in a dual cantilever mode with a constant stress of 12 MPa. In this study, the stress of 12 MPa was applied instantly and maintained for 30 minutes, and then released to allow specimen recovery for 90 minutes. Each creep test was replicated at least two times and then the average values were taken and recorded as the output response of each experimental run as per experimental design matrix. In this study, DMA was calibrated using standard steel sample provided by DMA manufacturer. It is very important to calibrate DMA machine prior conducting the experiments and the clamp compliance should be less than the value of 0.635 µm/ n (recommended value by TA instrument manufacturer). If the value of clamp compliance is more than 0.635 µm/ n or if the sample length is entered incorrect during the calibration stage the creep properties will be high even if the sample is very stiff. This can lead to inaccurate results.

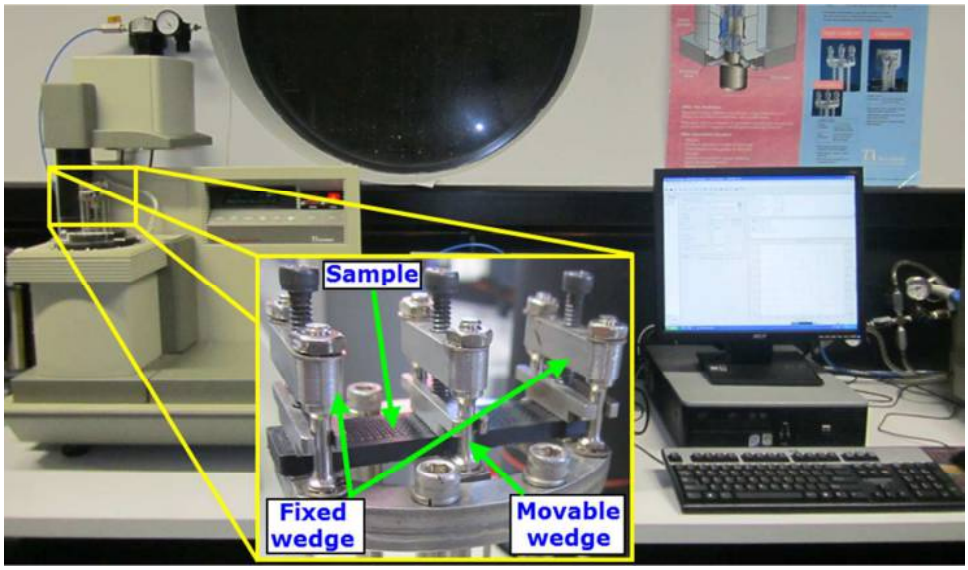

FIGURE 1. Method of clamping in single cantilever DMA device.

A typical creep and recovery curve is shown in Fig.2. Creep compliance is defined as the time-dependent strain per unit applied load. It is fundamental property of a material or structure that describes its behavior as a function of time along with two response functions - relaxation modulus and complex modulus. Recoverable compliance measures how well the material and part structure can return to its original shape and dimension after releasing the applied stress. The lower the recoverable compliance (i.e. low plastic deformation under load) is, the higher the elasticity of the sample is.

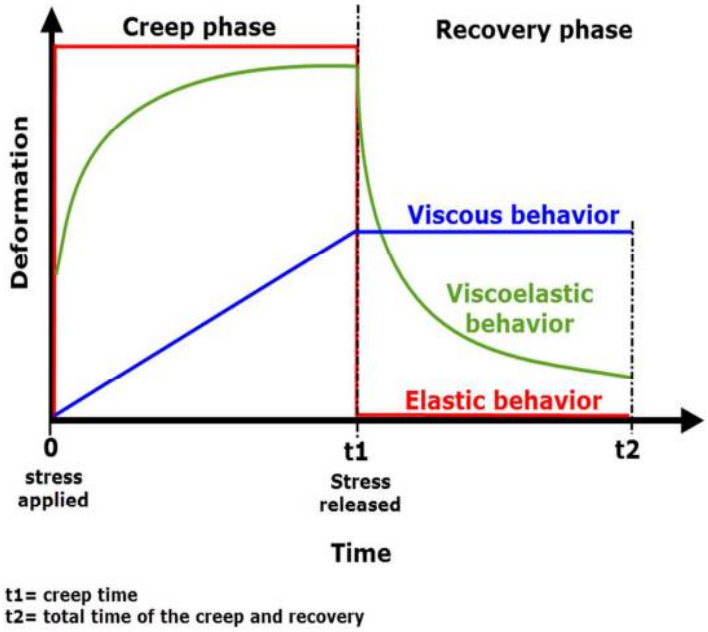

FIGURE 2. A typical creep and recovery behavior of elastic, viscoelastic and viscous materials

Definitive screening designs (DSD) are the new class of experimental designs that have three levels, which provide superior properties as compared to the traditional experimental design technique such as standard central composite designs in response surface methodology (Jones and Nachtsheim, 2011). DSDs are alternative one-step approach that is more reliable, efficient and cost effective than the conventional designs for problems involving up to 12 factors. These designs efficiently estimate the main effects, two factor interactions, and quadratic effects that are unbiased (not confounded) at minimum number of experiments (Jones and Nachtsheim, 2013). DSDs have the following advantage and desired properties over the classical experimental designs:

- Two-factor interactions are not aliased (not confounded) with higher order interactions.
- DSDs have distinctive feature that it is a self-foldover.
- DSDs can effectively separate the estimate of the nonlinear effect of each factor. Thus DSDs are capable to identify which factor is responsible for non-linearity.
- The number of required experiments is only one more than double the number of factors.
- The quadratic effects are estimable.

- With more than four factors, the DSDs provide higher level of statistical efficiency and able to conduct sensitivity analysis.

Since this paper presents for the first time the application of recently developed class of three level design - definitive screening designs - in the manufacturing processes, it is interesting to assess visually about what makes this design so distinct. Fig.3 shows correlation plot for the definitive screening design and fractional factorial design. In the correlation map for the fractional factorial design as shown in Fig.3 (a), it can be noted that all the cells are either pure blue or red indicating that the model terms are either completely uncorrelated or confounded, which means any important interaction terms will be bias (confound) with several main effects, causing the misleading results and unable to estimate the main effect correctly. Moreover, the block of red cells in the lower right side indicates that the quadratic effects are not estimable and they are confounded with each other. This design has some ability to identify strong nonlinear effect. However, it cannot identify which factor is causing the nonlinearity in the relationship. Therefore, traditional designs will require running further experiments to resolve the ambiguity. In contrast, the correlation map for the definitive screening design as shown in Fig.3 (b) indicates that the design allows estimating main effects, two-factor interactions and quadratic effects with a small increase in the variance. It can also be seen from Fig.3 (b) that all of the main effects are orthogonal to each other and with interactions and quadratic effects. It can also be seen that only slanting cells on the graph are pure red, which means that the model terms are not confounded (aliased) with each other. The quadratic effects are weakly correlated with each other and uncorrelated with the interaction effects. That means all quadratic effects can be estimated using definitive screening design.

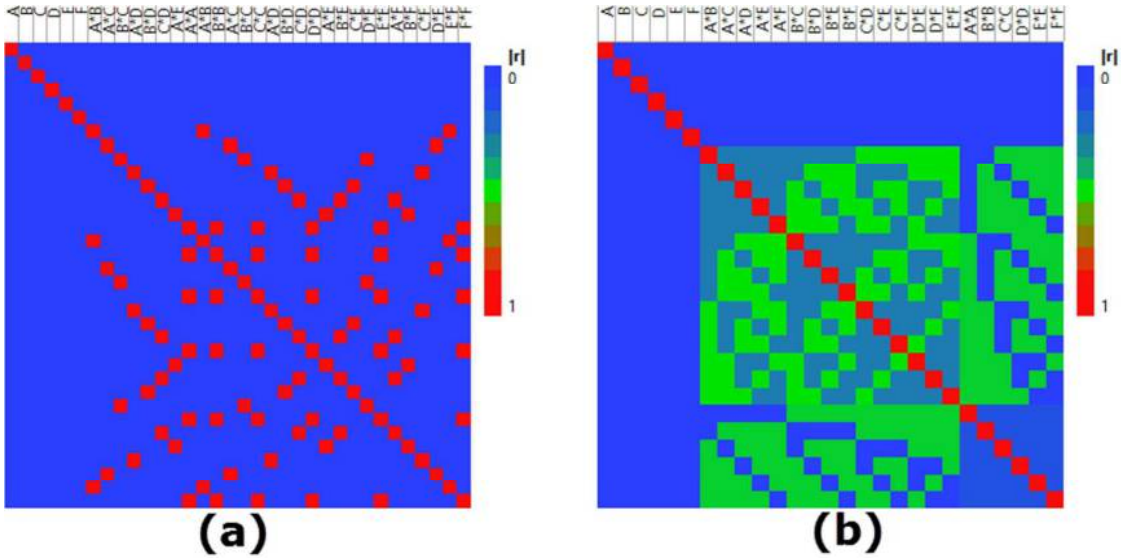

FIGURE 3. Color map for the: (a) the fractional factorial design, and (b) the definitive screening design.

In this study, six process parameters namely layer thickness (A), air gap (B), raster angle (C), build orientation (D), road width (E) were selected as shown in Table 1 and described in (Mohamed et al., 2015). Theses process parameters are selected because they have already been identified as the most significant FDM process parameters by several researchers (Brensons et al., 2015; Durgun and Ertan, 2014; Lanzotti et al., 2015; Mohamed et al., 2015; Onwubolu and Rayegani, 2014; Panda et al., 2009; Sahu et al., 2013; Sood et al., 2012a; Sood et al., 2009; Sood et al., 2010b; Sood et al., 2012b) in their studies of FDM process optimization and hence these parameters are considered in this paper to study their effects on the creep properties. The sixth parameter, the 'number of contours (F)' is also considered in this study along with five parameters. This variable affects the quality of strength of the layer around the raster beads and thus may affect the creep performance of fabricated part, and therefore it is a particular of interest to include this parameter in this study. Other process parameters are kept constant at their levels (Table 2). It is well known that the density of FDM printed part is determined by the variable part interior build style (Nuñez et al., 2015; The-Technology-House, 2015). The FDM Fortus 400 system has three different options for part densities or build styles (Chapman, 2014). Those are solid normal (100% filled the part), sparse low density (10% filled the part) and sparse high density (50% filled the part) (Nuñez et al., 2015; Stratasys, 2013). These options are shown in Fig.4. Solid normal fills the part with no gaps between raster legs for interior regions (Stratasys, 2015). Hence, it creates the part with maximum density. Sparse low density minimizes the amount of model material used to print the part as it creates some air gaps between part rasters. Thus, it builds the part much faster than solid – normal. However, sparse low density lacks the mechanical strength. While sparse high density is between solid- normal and sparse low density. It fills the part with an extra boundary contour. As a result, it prints the part with a balance between minimum amount of model material and mechanical properties. Although the interior build density is an important parameter having significant influence on the mechanical properties, the previous studies (Arivazhagan and Masood, 2012; Hopkinson et al.; Masood et al., 2010) reported that use of solid-normal gives the highest mechanical properties. This result is expected as solid normal fills the part completely with fully dense interior regions. Therefore, this study considers only solid normal part interior style and therefore relative density is assumed as constant because of its characteristics of having no micro-void structure which will make the printed part stronger and strengthen the material performance.

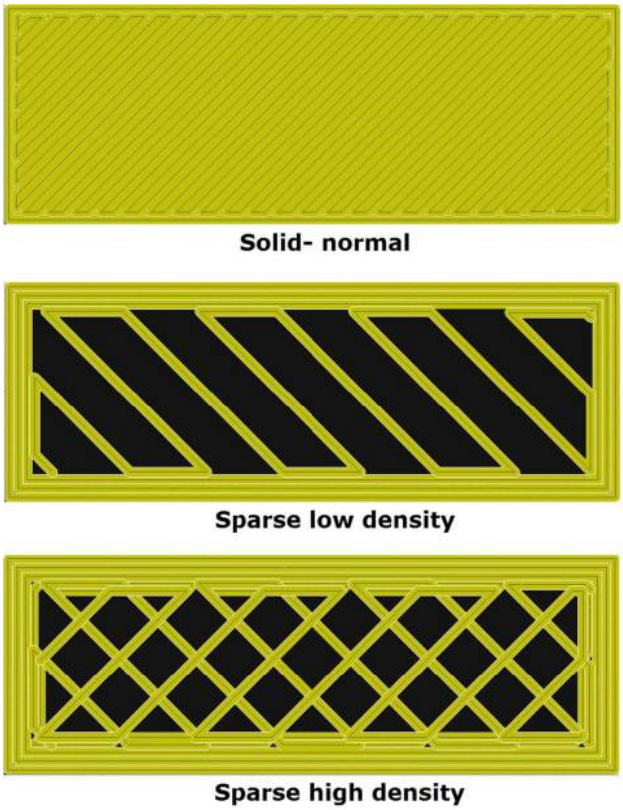

FIGURE 4. The variation in density between solid, low and high part interior fill.

The creep compliance and recoverable compliance were selected as the primary responses of interest. The DSDs require a minimum of $2k + 1$ runs, where k is the number of factors. Therefore, a study of six process parameters requires 13 experimental runs, which includes one center point. The design matrix was augmented with three additional replicate center points, resulting in a total of 16 runs (see Table 3) in order to improve the estimation of quadratic effects and experimental error. The process parameters selected in this study are shown graphically in Fig. 5.

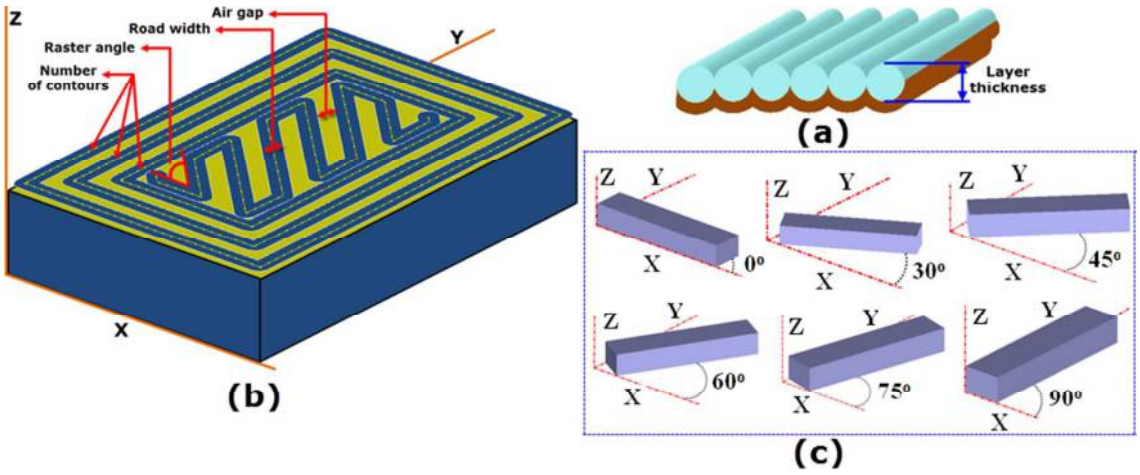

FIGURE 5. (a) layer thickness, (b) FDM tool path parameters, and (c) build orientations.

Table 1. Selected FDM process parameters and their levels

Factors	**Controllable factors**				
	Units	Symbols	Levels		
			Low	Center	High
Layer thickness	mm	A	0.127	0.254*	0.3302
Air gap	mm	B	0	0.25	0.5
Raster angle	deg	C	0	45	90
Build orientation	deg	D	0	45	90
Road width	mm	E	0.4572	0.5177	0.5782
Number of contours	-	F	1	5*	10

* modified level.

Table 2. Fixed factors and their levels

Factor	**Level**	**Unit**
Part interior density	Solid	-
Contour to contour air gap	0.0000	mm
Contour to raster air gap	0.0000	mm
Contour width	0.4572	mm
Part X Y shrink factor	1.0075	-
Part Z shrink factor	1.0070	-
Visible surface style	Normal	-

Table 3. Experimental design matrix

Run	A	B	C	D	E	F	Creep compliance ($\mu\mathbf{m^2/N}$)	Recoverable compliance ($\mu\mathbf{m^2/N}$)
1	-1	-1	-1	+1	0	+1	1330.624	1096.198
2	+1	0	-1	+1	+1	-1	3979.747	3009.447
3	-1	+1	0	+1	-1	-1	4950.958	4111.691
4	-1	+1	-1	-1	+1	0	2264.466	1945.186
5	-1	-1	+1	0	+1	-1	1489.022	1217.957
6	+1	+1	-1	0	-1	+1	2238.778	1645.631
7	0	-1	-1	-1	-1	-1	1561.136	1179.775
8	+1	+1	+1	-1	0	-1	6917.075	5058.596
9	-1	0	+1	-1	-1	+1	1411.272	1182.01
10	+1	-1	+1	+1	-1	0	1728.434	1232.326
11	0	+1	+1	+1	+1	+1	1689.031	1377.069
12	0	0	0	0	0	0	2224.664	1738.047
13	+1	-1	0	-1	+1	+1	1755.145	1263.024
14	0	0	0	0	0	0	2044.292	1671.334
15	0	0	0	0	0	0	2194.312	1685.341
16	0	0	0	0	0	0	2154.423	1698.241

3. Results and discussion

The response surface for creep compliance and recoverable compliance is a function of layer thickness (A), air gap (B), raster angle (C), build orientation (D), road width (E) and number of contours (F) which can be expressed as follows:

$$Y = \beta_0 + \sum_{i=1}^{k} \beta_i X_i + \sum_{i=1}^{k} \beta_{ii} X_i^2 + \sum_{i<j}^{k} \beta_{ij} X_i X_j + \varepsilon \qquad (1)$$

where Y denotes the predicted response, X_i and X_j are the coded variables, k is total number of variables, β_0 is the constant term of the regression equation, β_i is the linear coefficient, β_{ii} is the coefficient of the squared term of each variable, β_{ij} is the interaction coefficient, and ε is the random error, which contains measurement error and other variability.

Regressors with the highest partial probability values (P> 0.1) were excluded from the regression models using the backward elimination approach, as it improves the quality of fit for the experimental data. Based on the ANOVA results, the quadratic model was found to be appropriate for creep compliance and recoverable compliance (see Tables 4 and 5) with p-value less than 0.05 and lack of fit more than 0.05. The results also confirm that the developed regression models have 95% confidence level, and these models can be used for future application. The value of the coefficient of determination (R^2) also indicates the goodness of fit of the developed models. In this case, the value of the coefficient of determination (R^2) and the adjusted coefficient of determination (adjusted R^2) for both regression models are found to be high, which indicate that the developed regrssion models are adequate and highly significancnt for the models.

Table 4. ANOVA results for creep compliance

Source	DF	Sum of Squares	Mean Square	F Ratio
Model	9	34561263	3840140	767.4260
Error	6	30024	5004	**Prob > F**
C. Total	15	34591287	-	**<.0001***
Lack Of Fit	3	11369.770	3789.92	0.6095
Pure Error	3	18653.768	6217.92	**Prob > F**
Total Error	6	30023.537	-	0.6529
Summary of fit				
R^2				0.9991
R^2 Adj				0.9978

* High significant model (P <0.05)

Table 5. ANOVA results for recoverable compliance

Source	DF	Sum of Squares	Mean Square	F Ratio
Model	11	19567089	1778826	2401.712
Error	4	2963	741	**Prob > F**
C. Total	15	19570051	-	**<.0001***
Lack Of Fit	1	487.6829	487.683	0.5912
Pure Error	3	2474.9143	824.971	**Prob > F**
Total Error	4	2962.5972	-	0.4980
Summary of fit				
R^2				0.9998
R^2 Adj				0.9994

* High significant model (P <0.05)

The plot of the experimental values and the respective predicted values is shown in Fig. 6. From this graph it can be observed that the predicted response values are in good agreement with the experimental values, which indicates an adequate signal for the regression models. It does not show any unusual variance or lack of fit issues. Tables 6 and 7 show the estimated regression coefficients of model terms. From Tables 6 and 7, the most influencing parameters for creep complaince and recoverable complaince can be identified as compared to other parameters. These results indicate that the air gap has a postive effect on creep properties, while the number of contours has a negative effect on these properties.

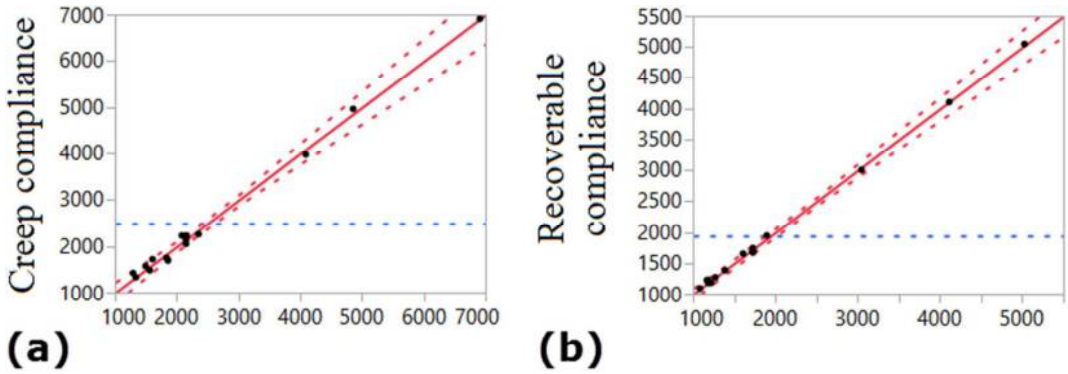

FIGURE 6. Comparisons of the predicted and experimental values for: (a) creep compliance, and (b) recoverable compliance.

Table 6. Estimated regression coefficients and their significance for creep compliance

Term	Estimate	Plot Estimate	Std Error	t Ratio	Prob>|t|
Intercept	1901.8687	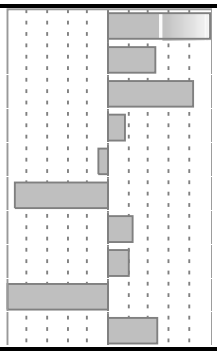	35.24599	53.96	**<0.0001***
A	540.0616		22.3199	24.20	**<0.0001***
B	979.72518		22.42986	43.68	**<0.0001***
C	197.71919		22.41485	8.82	**0.0001***
E	-111.1862		22.42986	-4.96	**0.0026***
F	-1061.388		22.41365	-47.35	**<0.0001***
A*B	281.58634		28.13761	10.01	**<0.0001***
C^2	236.79497		45.9759	5.15	**0.0021***
B*F	-1160.559		28.11761	-41.28	**<0.0001***
F^2	557.6538		44.46593	12.54	**<0.0001***

* High significant term (P <0.05)

Table 7. Estimated regression coefficients and their significance for recoverable compliance

Term	Estimate	Plot Estimate	Std Error	t Ratio	Prob>|t|
Intercept	1539.8094	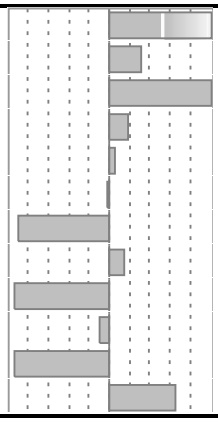	13.98475	110.11	**<0.0001***
A	265.10563		8.584663	30.88	**<0.0001***
B	848.23003		8.661964	97.93	**<0.0001***
C	152.51283		8.661964	17.61	**<0.0001***
D	53.154735		8.661964	6.14	**0.0036***
E	-20.53427		8.661964	-2.37	**0.0768**
F	-768.0127		8.661964	-88.66	**<0.0001***
A*B	123.31969		17.65813	6.98	**0.0022***
A*D	-790.1344		11.54629	-68.43	**<0.0001***
B*D	-76.62579		17.6842	-4.33	**0.0123***
C*E	-793.62		18.65758	-42.54	**<0.0001***
F^2	552.43351		19.20301	28.77	**<0.0001***

* High significant term (P <0.05)

The final response surface models for the responses are presented by Eqs.2 and 3.

$$Creep\ compliance\ (\mu m^2/N) = 1901.868 + 540.061 \times A + 979.725 \times B + 197.719 \times C + -11.186 \times E + -1061.388 \times F + 281.586 \times AB + 236.794 \times C^2 + -1160.559 \times BF + 557.653 \times F^2 \quad (2)$$

$$Recoverable\ compliance\ (\mu m^2/N) = 1539.809 + 265.105 \times A + 848.230 \times B + 152.512 \times C + 53.154 \times D + -20.534 \times E + -768.012 \times F + 123.319 \times AB + -790.134 \times AD + -76.625 \times BD + -793.620 \times CE + 552.433 \times F^2 \quad (3)$$

The main effects of processing parameters can be studied by the levels of averaging creep compliance and recoverable compliance of the raw data. The level average responses from raw data are useful to analyze and evaluate the trend of the creep behavior of the manufactured part with respect to the variation of the parameters. The lowest points of these

plots correspond to the optimum parameter stetting. The main effects of raw data are shown in Fig. 7 (a) for creep compliance and Fig. 7 (b) for recoverable compliance. Results presented in these figures indicate that the creep behavior of the built part is a parabolic function of the layer thickness, air gap, raster angle and the number of contours. If the value of compliance is too high, it means the elasticity of the part is too low at the forming force to maintain the desired shape.

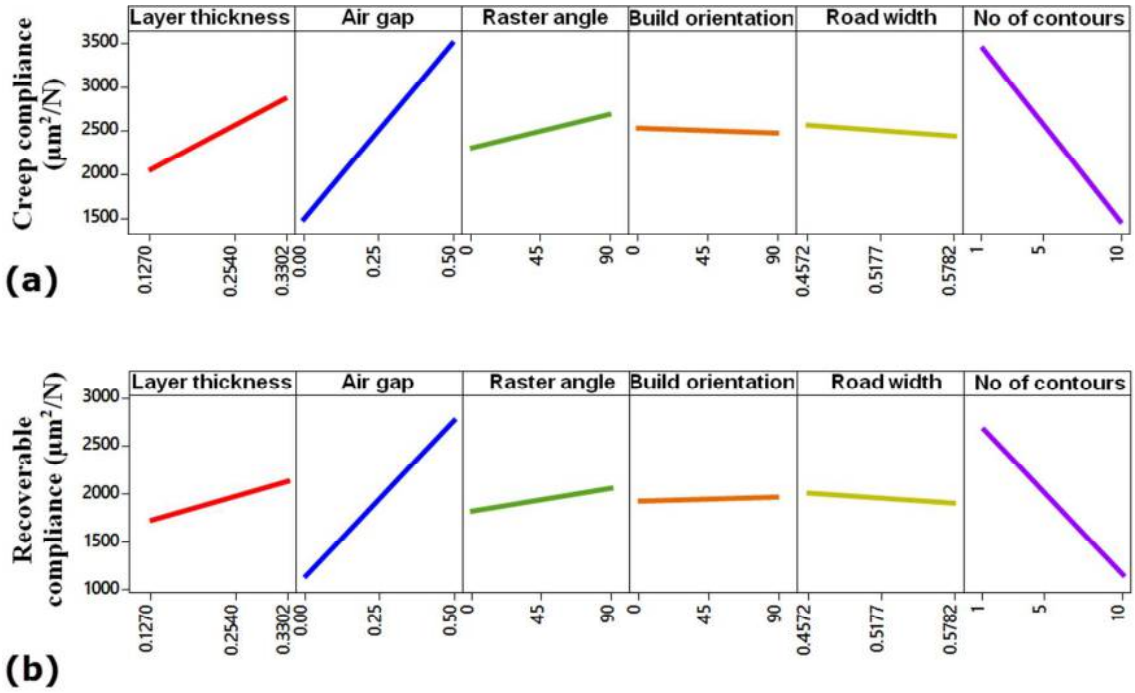

FIGURE 7. Effect of process parameters on (a) creep compliance, and (b) recoverable compliance.

It can be observed from Fig 7 (a and b) that with the increase in the layer thickness from 0.127 mm to 0.3302 mm, there is a gradual increase in creep compliance and recoverable compliance. Reducing the layer thickness to a lower value (0.127 mm) can also reduce staircase effects. The staircase effects cause voids between two rasters. These voids are formed at the intersection of the crosshatched regions, which cause air entrapment, and hence increase porosity. A lower value of layer thickness is found to be the optimum value to improve the creep resistance of the built part as it reduces these voids between the two rasters by decreasing the staircase error, thus eliminating the porosity also. Therefore, the manufactured parts with the lower value of layer thickness tend to have better creep resistance. Fig 7 (a) and (b) show that the air gap also has a significant effect on creep properties of the processed part. As the air gap increases, the creep compliance and recoverable compliance of the manufactured part increases. As the air gap is increased, the defect between rasters occurs as a void or unfilled spaces leading to weak interface bonding and brittle structure. Therefore, the manufactured part with a high value of air gap has a lower creep resistance than the manufactured part with no air gap. Raster angle has a significant

influence on the creep performance of the part. It can be seen from Fig 7 (a) and (b) that the creep compliance and recoverable compliance increased with the increase in raster angle from 0˚ to 90˚. This is due to the fact that the lower value of raster angle produces minimum number of raster, which is prone to minimum distortion in single layer. Moreover, a lower value of raster angle helps in obtaining smaller curves, and smaller sharp turns, hence incomplete filling between rasters can be reduced. If the sample is processed with higher value of raster angle (i.e., 45˚), then there will be some large pores and voids formed in interior structure (see Fig.8 (a)) which makes the part brittle and easy to fail in early stage of applying load.

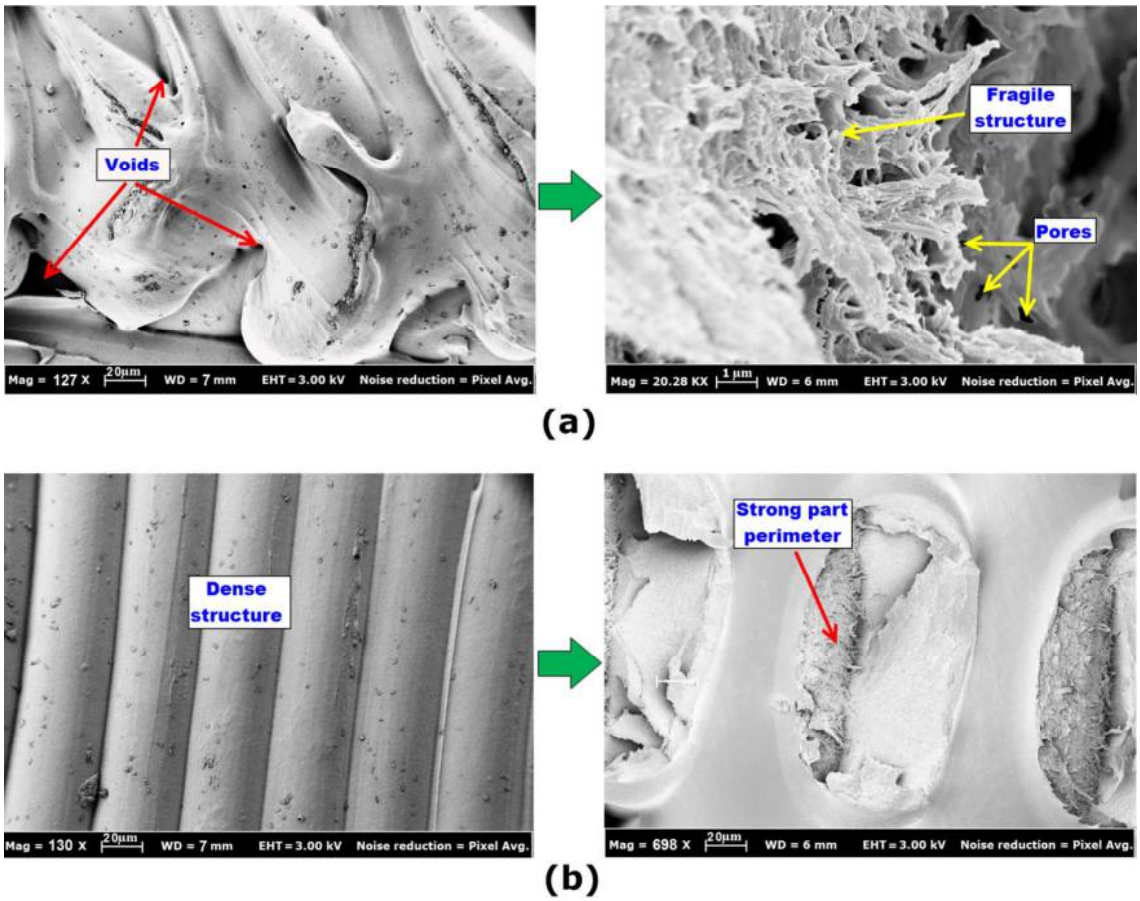

FIGURE 8. SEM images showing (a) air voids and pores in the part processed with raster angle of 45, and (b) part processed with 10 contours showing dense structure and strong perimeter.

Fig 9 is an interesting graph showing the comparison between raster angle of 0˚ and raster angle of 90˚ and their impacts on the creep performance. If the sample is processed with raster angle of 0˚ and is subjected to gradually increasing load, as shown in Fig. 9 (a), the applied load requires separating and fracturing a large number of plastic fibers and polymer chain molecules due to their parallel orientation and arrangement to the direction of loading. The ligament structures are particularly well-adapted to resist the deforming forces. The more extended the fibers are, the stronger is the ligament or tendon. These structures exhibit higher

stiffness (resistance to deformation), creep performance, and thus the manufactured part is able to regain its original shape after releasing the load. However, if the part is processed with raster angle of 90˚ as shown in Fig. 9 (b), the stress or load can break the part easily due to separation occurring at the interface of rasters and the part structure reaches the point of failure quickly. In this case, when the part is subjected to sudden, gradual, prolonged, or excessive loads, the part may exceed the maximum elastic limit. This leads to permanent deformation or rupture and the part will no longer be able to return to its original shape after removing the deforming force.

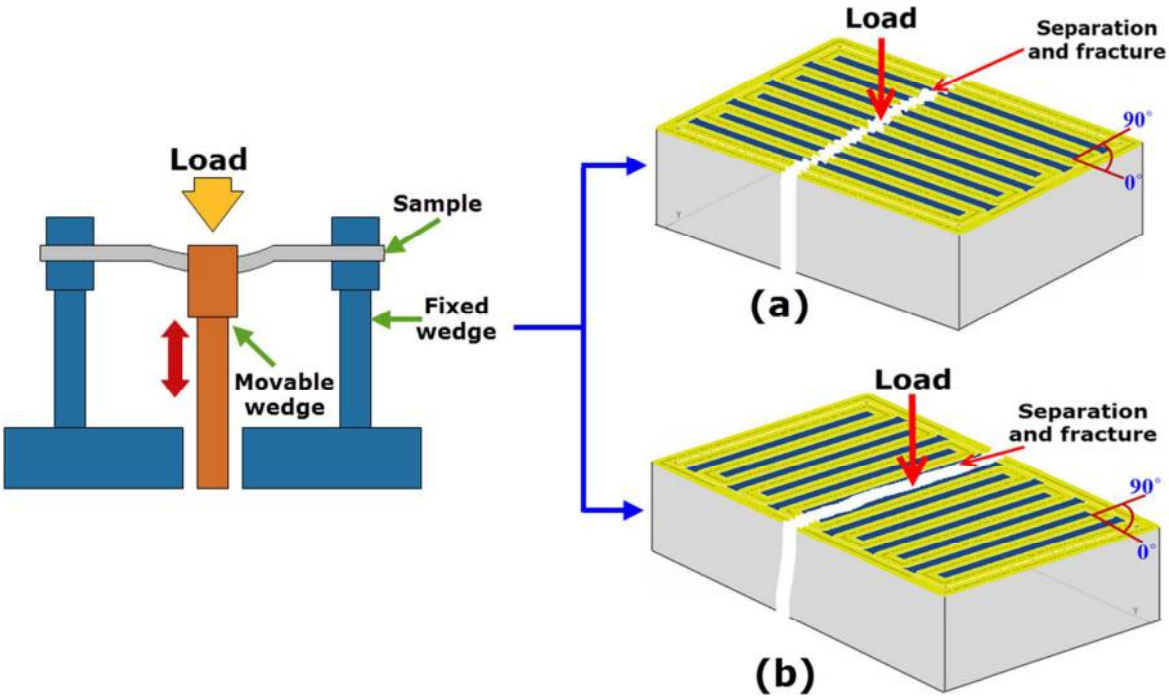

FIGURE 9. Failure on the specimen processed with (a) raster angle of 0˚, and (b) raster angle of 90˚.

Experimental results show that build orientation has a very marginal effect on the creep behavior of the part as shown in Fig 7 (a) and (b). However, it has a significant interaction effect on the recoverable compliance as can be seen in Table 7. But the decrease in the build orientation from 0˚ to 90˚ helps in obtaining better part structure for creep performance because it reduces stair-stepping imperfection effect and therefore incomplete filled area can be minimized. It can also be seen from Fig 7 (a) and (b) that the road width has a marginal effect on the creep compliance and recoverable compliance. However, the increase in road width from 0.4572 mm to 0.5782 mm helps to improve the creep performance. A possible explanation for this effect is that higher road width reduces voids in the sub-perimeter region, thus reducing the porosity. Furthermore, a higher value of road width requires fewer loops to fill interior area, which is subject to less time for single layer deposition, leads to a more uniform nozzle speed and uniform temperature resulting in minimum distortion. Therefore, it

helps in improving the creep resistance and the part can regain its original state when the deforming force is released.

Number of contours also found to be the most effective parameter affecting the creep properties of the manufactured part. It should be noted here that the default machine setting for this factor is a single contour. However, the results plotted in Fig 7 (a) and (b) show that the creep performance of the processed part can be improved significantly by setting-up this factor at its highest level (10 contours). This is due to the fact that the number of contours builds stronger part walls, which increases its energy absorption because the applied stress or load in this case is carried by the contours instead of rasters. These contours store the energy and keep it available, which enables the part to revert to its original dimension after removing the deforming load. Besides, the higher number of contours decreases the number of rasters and raster length, resulting in reduction of the formation of voids or porosity (see Fig. 8 (b)) at the intersection of the crosshatched regions. Hence a dense structure for manufactured part can be obtained and the part exhibits the property of viscoelasticity. This helps the part to be purely elastic, thus the part can recoil back to its original position after removal of the deforming force without changing the shape or becoming crooked and distorted. Fig. 10 also illustrates the comparison results between the specimen fabricated with the highest number of contours and with single contour.

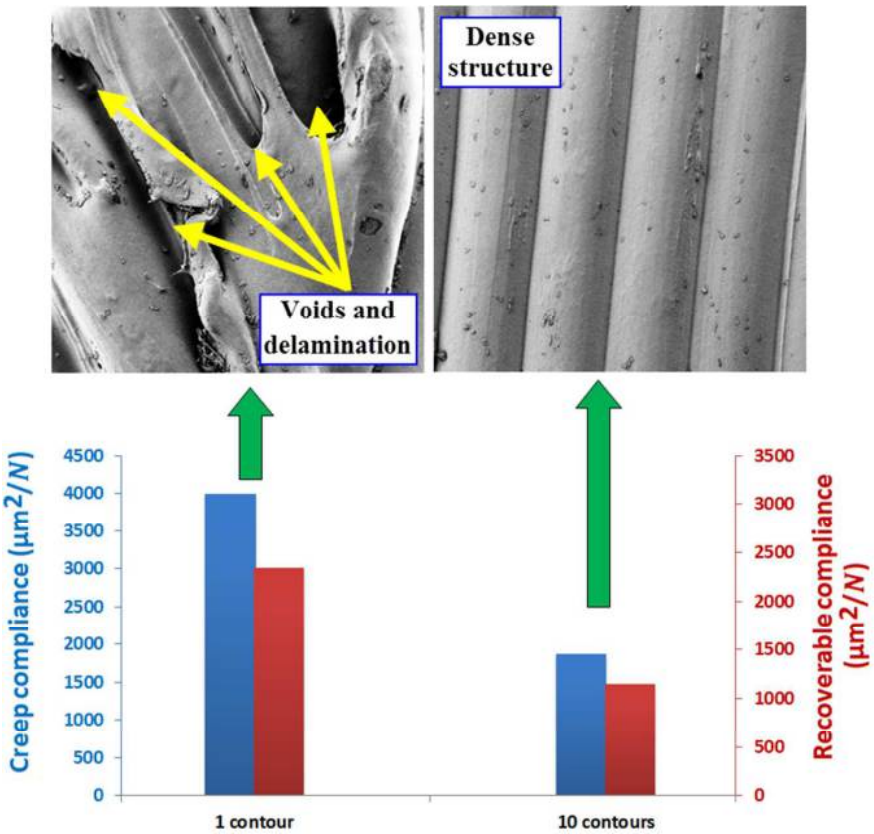

FIGURE . 10. Effects of number of contours on Creep performance of the manufactured part.

A significant interaction effect between some process parameters for creep compliance and recoverable compliance was also observed. The 3D response surface plots for significant interactions between process parameter are shown in Fig. 11 (a) to (d). Fig. 11 (a) and (b) reveal that, as layer thickness and air gap increased from low level to the higher level, it results in gradual increase in creep compliance and recoverable compliance. Fig. 11 (c) shows that recoverable compliance has improved with decrease in layer thickness and increase in build orientation. However, this figure shows that recoverable compliance can also be improved by using the higher value of layer thickness and lower value of build orientation. The interaction between raster angle and road width can be seen in Fig. 11 (d). This figure shows that increase in raster angle results in poor recoverable compliance. A similar trend has also been observed in case of road width. The rate of recovery of the part to its original shape is high if the part is processed with the highest value of road width.

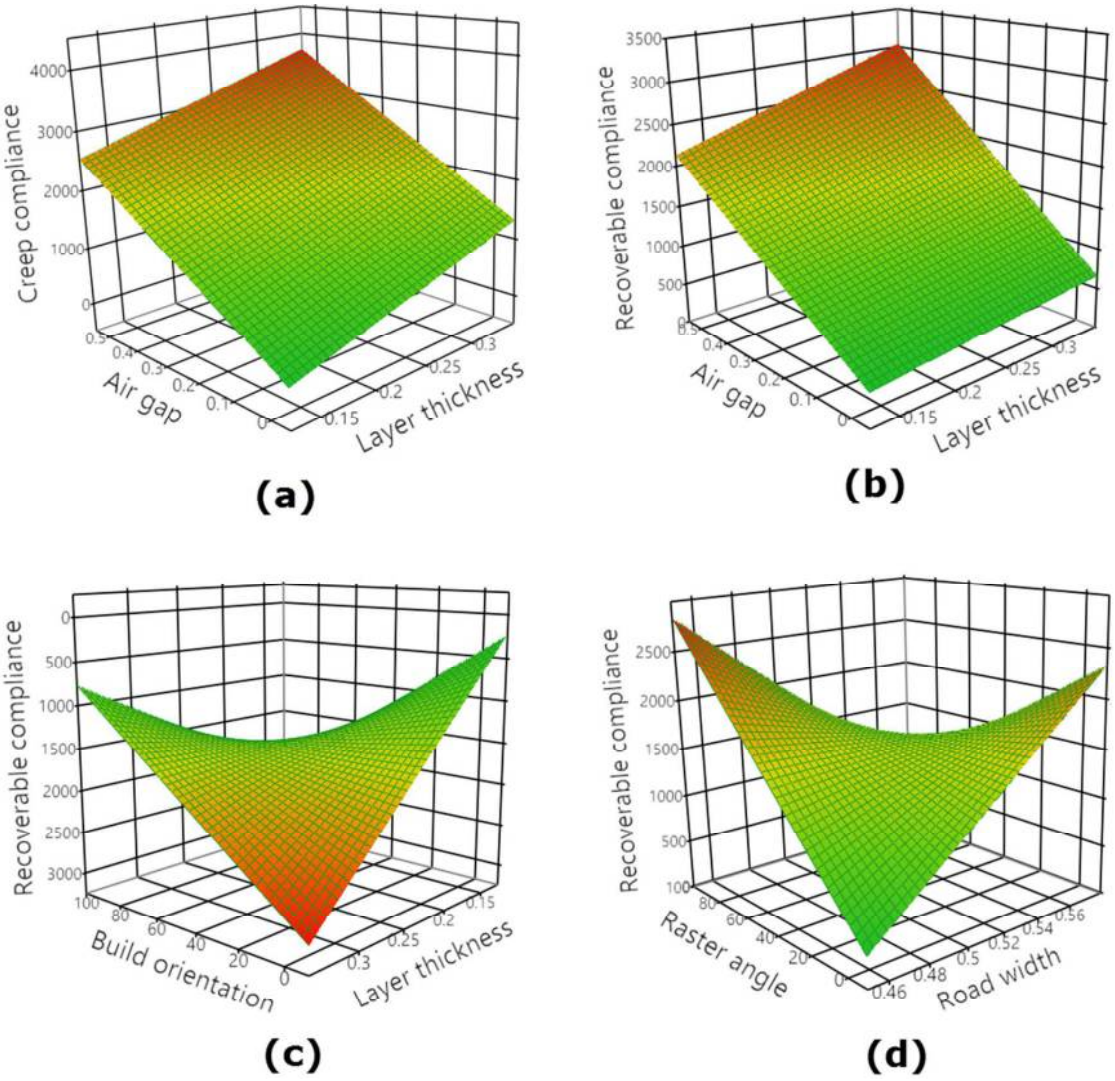

FIGURE 11. 3D response surface plots showing the effect of different interaction parameters: (a) air gap and layer thickness on the creep compliance, (b) air gap and layer thickness on the recoverable compliance, (c) build orientation and layer thickness on the recoverable compliance, and (d) raster angle and road width on the recoverable compliance.

4. Multilayer Perceptron Neural Network (MMLP)

Since the FDM process has a complex mechanism of manufacturing part with a large number of intervening parameters, the standard techniques for optimization are not effective especially if there is more than one response variable. Therefore, the artificial neural network (ANN) is an alternative modelling technique that is based on the biological neural network, such as the brain and it is commonly used in many research fields such as control, data compression, prediction, optimization, pattern recognition, classification and regression (Towell and Shavlik, 1994). The ANN model considered in this study is a Multi-Layer Perceptron (MLP) model. A MLP model comprises of an input layer, a hidden layer and an output layer. Process parameters are described by neuron and thus the input layer has six neurons (six process parameters). The hidden nodes produce various mathematical relationships (Hammerstrom, 1993). The number of hidden nodes was determined by testing a different ANN structures under various number of neurons in the hidden layer. After data training, the topology 6-10-2 was selected as the optimum structure based on the minimum error. The output layer reports the creep compliance and recoverable compliance values to train the ANN in order to determine the relationships between the input and output variables. A neural network was configured with a Kfold value of 5 for validation. Kfold cross validation divides the experimental data into K subsets and each of the K subsets is then used to confirm and validate the quality of fit for the model based on the rest of the data (Kohavi, 1995). Kfold cross validation method is best for the problems with small data, as it makes efficiency and reliability with limited data. The model provides the best validation statistic was selected as the final model. The penalty method 'Square root penalty' is used in this study because all process parameters contributed to the predictive ability of the models. The square root penalty can be expressed by Eq.4. Fig. 12 schematically shows the ANN architecture used in this study.

$$\text{SRP} = \sum \beta_i^2 \qquad (4)$$

where SRP denotes Square Root Penalty which is the penalty parameter, and $\sum \beta_i^2$ is the function of the parameter estimates.

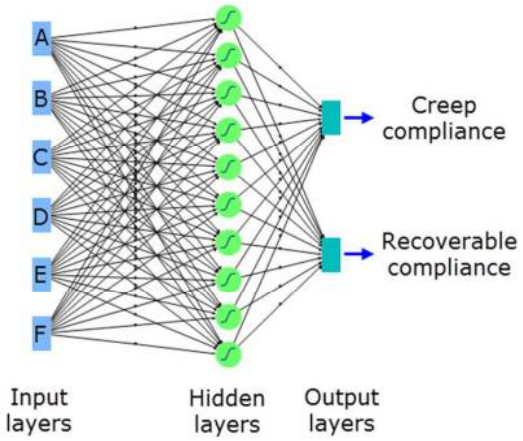

FIGURE 12. Design of neural network architecture

Fig. 13 shows the comparison between the experimental values, ANN predictions and DSD predictions for the two responses. The preliminary results presented in Fig.13 show that high (R^2) values occur for developed models using both ANN and DSD, demonstrating that the models are predicting well. It can also be seen from this figure that the predicted values are in very good agreement with the experimental values. The proposed ANN and DSD have the modeling competence with average accordance ratio of almost 99.69 %. Since DSD is a new class of experimental design and has not been applied in manufacturing processes before, our findings indicate that DSD can fit the quadratic model well with a minimum number of runs and it has better ability for prediction.

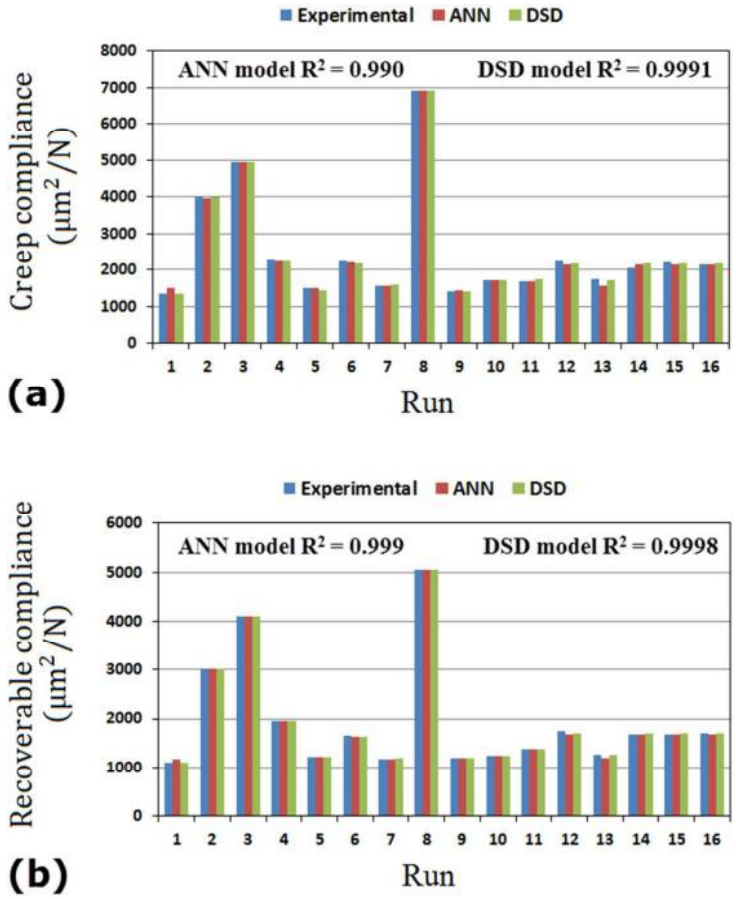

FIGURE 13. Comparison between experimental values, ANN prediction and DSD prediction for (a) creep compliance, and (b) recoverable compliance.

Desirability function based on neural network models was used in this study to obtain the minimum creep compliance and maximum recoverable compliance simultaneously. In the desirability function, each response of y was converted to an individual desirability function d that ranges from 0 to 1. The desirability function 'minimum-the-better' criteria is used to minimize the creep compliance and the recoverable compliance as expressed in Eq. (5) (Dodson et al., 2014).

$$d = \begin{cases} 1 & y < T \\ \left(\frac{U-y}{U-T}\right)^r & T \le y \le U \\ 0 & y > U \end{cases} \qquad (5)$$

where y is the response to be optimized, U is the upper limit, T is the target, and r is a weight factor.

Then the optimal parameter settings for creep compliance and recoverable compliance were obtained by maximizing the overall desirability$D$, which is the geometric mean of all the individual desirability functions as given in Eq. (6) (Vining, 1999).

$$D = (d_1 \times d_2 \times d_3 \ldots \times d_n)^{\frac{1}{n}} = \left(\prod_{i=1}^{n} d_i\right)^{\frac{1}{n}}, \qquad (6)$$

where, D is the overall desirability, n is the number of responses in the measure and $d_1, d_2, d_3 \ldots d_n$ are the individual desirability for a single response.

Once the optimum process settings are determined, as shown in Fig.14, through simulation, the final step is to confirm the optimal process settings for the predicted responses. Therefore, three additional samples were manufactured. The average values of the results from the confirmation experiments using optimized process parameters were compared with the predicted values as shown in Table 8. The percentage of prediction error was calculated by Eq. (7).

$$\text{Prediction error (\%)} = \left|\frac{\text{Actual value} - \text{Predicted value}}{\text{Predicted value}}\right| \times 100 \qquad (7)$$

It can be observed from Table 8 that the error between the actual results and predicted values lies between 2.74 % and 5.2. Thus the prediction performance of the models is quite satisfactory and can be used for future application.

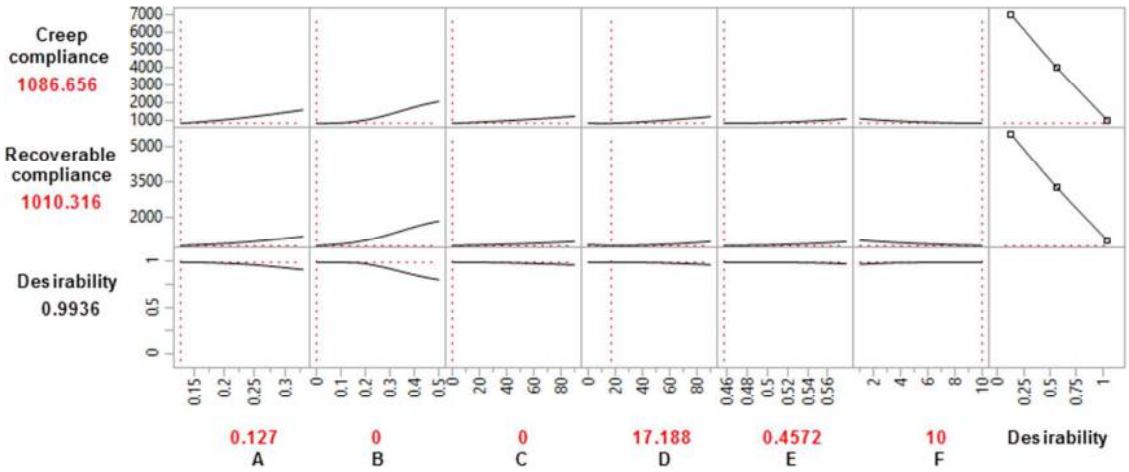

FIGURE 14. Desirability profiler showing the optimal parameter settings for two responses.

Table 8. Comparison between experimental and predicted values for the optimum parameter settings.

Response	Optimum parameter settings						Predicted values	Actual values	Error (%)
	A	B	C	D	E	F			
Creep compliance ($\mu\mathbf{m^2/N}$)	0.127	0	0	17.188	0.4572	10	1086.656	1116.379	2.74
Recoverable compliance ($\mu\mathbf{m^2/N}$)							1010.316	1063.21	5.2

After determining the optimum process parameters and predicting the responses under those parameters, new experiments were designed and conducted with the optimum levels of the process conditions in order to validate the improvement of creep properties on relatively complex parts. In this study, additional 4 samples contained complex features were fabricated on the same FDM system and using the same material. After manufacturing the test specimens, the creep tests were performed three times following similar method as discussed in section 2 and the average value of creep properties were computed. The confirmation experiments were carried out by setting the process parameters at the optimum levels. Two of these samples were fabricated with optimized process parameters. Other two samples were fabricated with un-optimized process parameters (default machine setting) in order to compare between optimized and un-optimized process parameters. Based on the experimental confirmation results presented in Fig 15, it is clear that the improvement of the creep properties from un-optimized process conditions (the default machine setting) to the optimized process parameter combination is high. Hence, the creep properties for different part shapes processed by FDM are improved significantly by using the optimal condition. The experimental results obtained through confirmation tests approve the validity, effectiveness and efficiency of optimal process setting derived by definitive screen design and ANN. It should be noted that if dynamic mechanical analyzer has improper calibration of the clamp for mass and compliance or entered an incorrect sample length, it will result in a high value for the compliance calculation. High compliance can lead to high creep rates for stiff materials or stiff part structure. Therefore, it is recommended to use maximum compliance value of 0.635 μm/ n. In this study, all creep experiments were conducted at the compliance value of 0.221 μm/ n. Future studies on creep properties of FDM printed part are necessary to investigate the effect of process parameters on other sample geometries contained complex features with different materials.

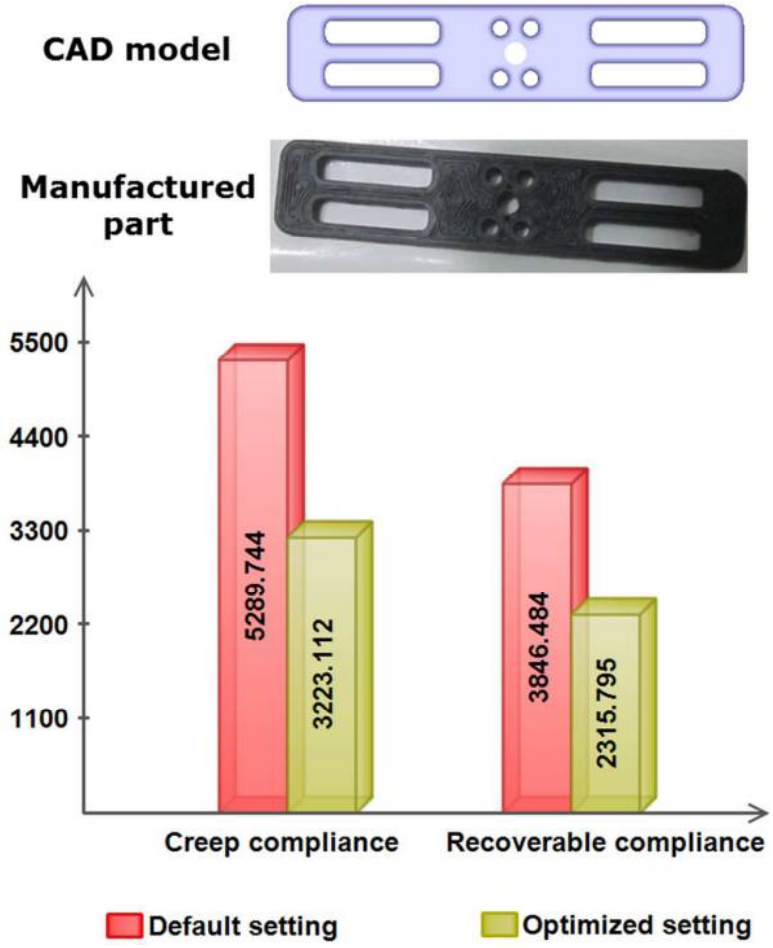

Figure 15: Illustrative comparison between optimized and default process settings.

5. Concluding remarks

In this study, an attempt has been made to develop empirical relationship between process parameters and creep performance of FDM manufactured parts using definitive screen designs and ANN, which is shown to overcome limitations of the previous studies. From the findings of the current study the following conclusions can be made:

1. This investigation has presented for the first time the application of definitive screening design to develop empirical models to predict and describe the creep properties of manufactured parts by FDM in terms of layer thickness, air gap, raster angle, build orientation, road width and number of contours. The results have proven that definitive screening design is an efficient design to identify the main effects, two factor interaction effects and quadratic effects obviated to run further experiments. This reduces the number of experiments from ≥ 50 runs to just 16 runs in the case of using standard screening and response surface designs. This is extremely useful especially in advanced manufacturing process which involves large number of intervening process parameters.

2. Layer thickness, air gap, raster angle and number of contours play significant roles in controlling the structure and creep performance improvement of FDM processed parts.

3. The increase in layer thickness (0.127 mm to 0.3302), air gap (0 mm to 0.5 mm) and raster angle (0˚ to 90˚), resulted in poor creep properties for the manufactured part, while the increase in number of contours (1 to 10) improves the creep performance significantly.

4. The lower level of build orientation and road width resulted in better creep properties and ability of the part to recoil its original shape after removing the deforming load. However, when the level of these parameters increases a continuing increase in recoverable compliance was observed.

5. The optimization process was conducted using desirability function based on the neural network, which can be applied to nonlinear and multitudinous problems. From the results obtained by ANN, it can be concluded that the optimum parameter settings to improve the creep performance and properties of the manufactured part are layer thickness = 0.127 mm, air gap = 0.00 mm. raster angle = 0˚, build orientation = 17.1880˚, road width = 0.4572 mm and number of contours = 10.

6. The findings of this study would help the future researchers and additive manufacturing process users to become more aware on how FDM process parameters influence the creep properties and recoverability of the manufactured parts. Moreover, the present methodology based on definitive screening design and neural network can open new opportunities for industry and future researcher to characterize the influence of processing parameters on the part properties for other advanced manufacturing technologies and problems involving with a wide range of process parameters. The empirical models developed in this study could help the designers in selecting the optimum process settings and desired creep properties.

References

Arivazhagan, A., and S. Masood. 2012. Dynamic mechanical properties of ABS material processed by fused deposition modelling. *Int J Eng Res Appl*. 2:2009-2014.

Brensons, I., S. Polukoshko, A. Silins, and N. Mozga. 2015. FDM Prototype Experimental Research of Processing Parameter Optimization to Achieve Higher Tensile Stress. *In* Solid State Phenomena. Vol. 220. *Trans Tech Publ*. 767-773.

Chapman, B. 2014. Increasing Toughness of 3D-Printed Plastic using Acetone Vapor. Wordpress.Available from < https://benchapman4.wordpress.com/2014/05/08/increasing-toughness-of-3d-printed-plastic-using-acetone-vapor/>.

DMA2980. 2002. Dynamic Mechanical Analysis. Operator's Manual. TA Instrument, New Castle. 4-8.

Dodson, B., P. Hammett, and R. Klerx. 2014. Probabilistic Design for Optimization and Robustness for Engineers. John Wiley & Sons.

Durgun, I., and R. Ertan. 2014. Experimental investigation of FDM process for improvement of mechanical properties and production cost. *Rapid Prototyping Journal*. 20:228-235.

Gajdoš, I., Ľ. Kaščák, E. Spišák, and J. Slota. 2015. Flexural Properties of FDM Prototypes Made with Honeycomb and Sparse Structure. *In Key Engineering Materials*. Vol. 635. Trans Tech Publ. 169-173.

Hammerstrom, D. 1993. Working with neural networks. *Spectrum, IEEE*. 30:46-53.

Hopkinson, N., R. Hague, and P. Dickens. Rapid manufacturing: an industrial revolution for the digital age, 2006. Wiley, ISBN: 0-470-01613-2. 139-140.

Impens, D., and R. Urbanic. 2015. Assessing the Impact of Post-Processing Variables on Tensile and Compression Characteristics for 3D Printed Components. *IFAC-PapersOnLine*. 48:652-657.

Jones, B., and C.J. Nachtsheim. 2011. A class of three-level designs for definitive screening in the presence of second-order effects. *Journal of Quality Technology*. 43:1-15.

Jones, B., and C.J. Nachtsheim. 2013. Definitive Screening Designs with Added Two-Level Categorical Factors. *Journal of Quality Technology*. 45:121-129.

Kohavi, R. 1995. A study of cross-validation and bootstrap for accuracy estimation and model selection. *In Ijcai*. Vol. 14. 1137-1145.

Lanzotti, A., M. Grasso, G. Staiano, M. Martorelli, E. Pei, and R.I. Campbell. 2015. The impact of process parameters on mechanical properties of parts fabricated in PLA with an open-source 3-D printer. *Rapid Prototyping Journal*. 21.

Masood, S. 2007. Application of fused deposition modelling in controlled drug delivery devices. *Assembly automation*. 27:215-221.

Masood, S.H., K. Mau, and W. Song. 2010. Tensile Properties of Processed FDM Polycarbonate Material. *In* Materials Science Forum. Vol. 654. Trans Tech Publ. 2556-2559.

Mohamed, O.A., S.H. Masood, and J.L. Bhowmik. 2015. Optimization of fused deposition modeling process parameters: a review of current research and future prospects. *Advances in Manufacturing*. 3: 42-53.

Onwubolu, G.C., and F. Rayegani. 2014. Characterization and Optimization of Mechanical Properties of ABS Parts Manufactured by the Fused Deposition Modelling Process. *International Journal of Manufacturing Engineering*. 2014.

Panda, S.K., S. Padhee, S. Anoop Kumar, and S. Mahapatra. 2009. Optimization of fused deposition modelling (FDM) process parameters using bacterial foraging technique. *Intelligent information management*. 1:89.

Peng, A., X. Xiao, and R. Yue. 2014. Process parameter optimization for fused deposition modeling using response surface methodology combined with fuzzy inference system. *The International Journal of Advanced Manufacturing Technology*. 73:87-100.

Sahu, R.K., S. Mahapatra, and A.K. Sood. 2013. A Study on Dimensional Accuracy of Fused Deposition Modeling (FDM) Processed Parts using Fuzzy Logic. *J. Manuf. Sci. Prod*. 13:183-197.

Sood, A.K., A. Equbal, V. Toppo, R. Ohdar, and S. Mahapatra. 2012a. An investigation on sliding wear of FDM built parts. *CIRP Journal of Manufacturing Science and Technology*. 5:48-54.

Sood, A.K., R. Ohdar, and S. Mahapatra. 2009. Improving dimensional accuracy of Fused Deposition Modelling processed part using grey Taguchi method. *Materials & Design*. 30:4243-4252.

Sood, A.K., R. Ohdar, and S. Mahapatra. 2010a. A hybrid ANN-BFOA approach for optimization of FDM process parameters. *In* International Conference on Swarm, Evolutionary, and Memetic Computing. Springer. 396-403.

Sood, A.K., R. Ohdar, and S. Mahapatra. 2010. Parametric appraisal of mechanical property of fused deposition modelling processed parts. *Materials & Design*. 31:287-295.

Sood, A.K., R.K. Ohdar, and S.S. Mahapatra. 2012b. Experimental investigation and empirical modelling of FDM process for compressive strength improvement. *Journal of Advanced Research*. 3:81-90.

Stratasys. 2013. FDM Insight software 9.1 user guide.

Stratasys. 2015. FDM BEST PRACTICE. Creating Variable Density Parts. Available from < http://usglobalimages.stratasys.com/Main/Files/Best%20Practices_BP/BP_FDM_VariableDensity_1215.pdf?v=635967464236479750>.

The-Technology-House. 2015. What FDM Part Density is Best for You? . Available from <http://www.tth.com/fdm-part-desnity-best/>.

Towell, G.G., and J.W. Shavlik. 1994. Knowledge-based artificial neural networks. *Artificial intelligence*. 70:119-165.

Vining, G. 1999. Statistical Process Monitoring and Optimization. CRC Press.